A Direct Calibration Algorithm for ADC Interleaving

Chi-kwan Chan, ^{1,2,3} Hina Suzuki, ^{1,4} David Forbes, ¹ Andrew Thomas West, ¹ Arash Roshanineshat, ^{5,1,4} Daniel P. Marrone, ¹ and Amy Lowitz ¹

Steward Observatory and Department of Astronomy, University of Arizona, 933 N. Cherry Ave., Tucson, AZ 85721, USA
 Data Science Institute, University of Arizona, 1230 N. Cherry Ave., Tucson, AZ 85721, USA
 Program in Applied Mathematics, University of Arizona, 617 N. Santa Rita, Tucson, AZ 85721, USA
 Department of Electrical and Computer Engineering, University of Arizona, 1230 E. Speedway Blvd., Tucson, AZ 85721, USA
 Texas Instruments Inc, 251 S Williams Blvd, Tucson, AZ 85711, USA

ABSTRACT

We introduce a novel direct calibration algorithm to address phase delay, gain, and offset mismatches in Analog-to-Digital Converter (ADC) time interleaving systems. These mismatches, common in high-speed data acquisition, degrade system performance and signal integrity, particularly in applications such as radio astronomy and very long baseline interferometry (VLBI). Our proposed algorithm uses a sinusoidal reference signal and Fourier analysis to isolate and correct each type of mismatch, providing a computationally efficient solution. Extensive numerical simulations validate the algorithm's effectiveness and demonstrate its ability to significantly enhance signal reconstruction accuracy compared to existing methods. This work provides a robust and scalable solution for maintaining signal fidelity in interleaved ADC systems and has broad applications in fields that require high-speed data acquisition.

Keywords: instrumentation: detectors—methods: numerical

1. INTRODUCTION

The accurate conversion of analog signals to digital is fundamental for a wide range of scientific and engineering applications, including radio astronomy (Iguchi et al. 2003; Dewdney et al. 2009; Event Horizon Telescope Collaboration et al. 2019a,b; Jiang et al. 2020; Event Horizon Telescope Collaboration et al. 2022), telecommunications, medical imaging, and various other scientific and industrial fields. This conversion is carried out by Analog-to-Digital Converters (ADCs), which sample continuous-time signals and convert them into discrete-time digital values. To achieve high sampling rates and enhance time resolution, many modern systems (e.g., Fuj 2010; Patel et al. 2014) employ ADC time interleaving—a technique in which multiple ADCs operate in parallel, each sampling the input signal at staggered intervals. By combining the outputs of these interleaved ADCs, the effective sampling rate is increased, thereby enhancing the overall performance of the system.

Despite its advantages, ADC interleaving introduces challenges due to mismatches among the interleaved ADCs. These mismatches can distort the signal and introduce spurious tones in the reconstructed signal (Elbornsson et al. 2005; Roshanineshat 2023). In VLBI systems, such as the Event Horizon Telescope (EHT)'s digital backend, these interleaving mismatches have been shown to produce persistent spectral artifacts that de-

grade signal fidelity and interfere with the detection of weak astronomical signals (see, e.g., Patel et al. 2014). Addressing these mismatches is critical for maintaining signal integrity and achieving the desired system performance.

Several calibration techniques have been proposed to mitigate the effects of these mismatches (e.g., Reeder et al. 2005; Manganaro & Robertson 2015; Shen et al. 2022; Sjöland & Palm 2022; Hu & Yi 2022; Sundström et al. 2023). While these methods have demonstrated success in correcting certain types of mismatches, many systems still face challenges in achieving robust, high-fidelity performance across all mismatch types.

In this paper, we introduce a novel direct calibration algorithm designed to correct phase delay, gain, and offset mismatches in ADC interleaving systems. Our approach leverages the elegant properties of the Fourier transform to simultaneously isolate and solve for each type of mismatch. This process is computationally efficient and highly effective, making it suitable for high-speed signal processing applications such as VLBI, where real-time calibration is crucial to preserving signal integrity over extended observation periods.

The paper is organized as follows. In section 2, we define the setup and notations used throughout the paper. In section 3, we derives the mathematical identities that form the foundation of our direct calibration algorithm. We describe the minimal sampling requirement and explore the algorithm's convergence properties in

sections 4 and 5. In section 6, we present the pseudocode that can be directly used in practical systems. Finally, we conclude the paper in section 7, summarizing our contributions and discussing their potential applications.

2. SETUP AND NOTATIONS

We consider a generic setup involving P identical ADCs, which we label as ADC_0 , ADC_1 , ..., ADC_{P-1} . Each ADC has a sampling interval of Δ , resulting in an individual sampling rate of $1/\Delta$. To achieve a higher effective sampling rate, we stagger the sampling times of these ADCs. Specifically, ADC_p samples the input signal with an additional temporal offset of $p\Delta/P = p\delta$, where $\delta \equiv \Delta/P$.

By interleaving the ADCs, the system samples the input signal at the following times:

$$t_{p,n'} \equiv n'\Delta + p\,\delta. \tag{1}$$

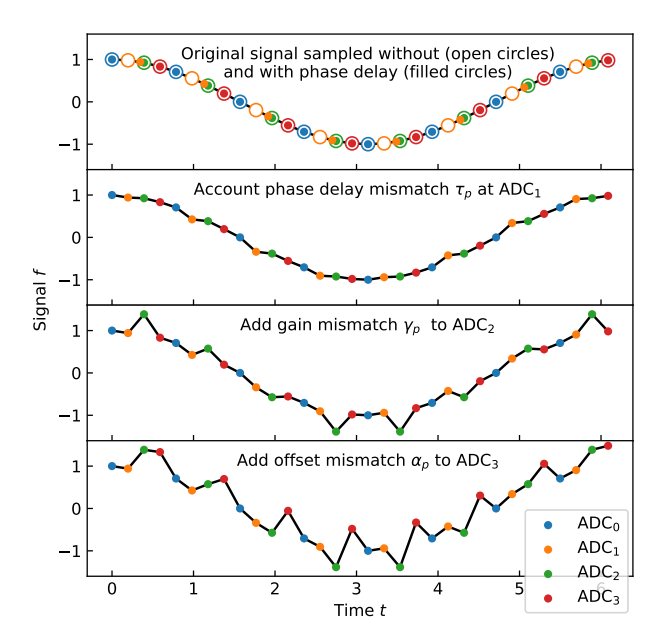


Figure 1. Illustration of the impact of mismatches in a 4-ADC interleaving system. The black solid curve in the shows the input signal. Open circles mark the ideal sampling points for a mismatch-free system, while filled circles show the actual sampling locations when mismatches are present. The top panel shows the ideal case so the black curve is $\cos(t)$. We introduce a phase delay mismatch, which samples the signal in a non-uniform fashion. The second panel highlights the effect of a phase delay mismatch in ADC₁, which results in a distortion in the reconstructed signal. The third panel adds a gain mismatch in ADC2, further modifying the amplitude of the sampled signal. The fourth panel introduces an offset mismatch in ADC₃, demonstrating how combined mismatches lead to significant distortion. Accurate calibration of these mismatches is essential for high-fidelity signal reconstruction in interleaved ADC systems.

Sorting these sampling times in ascending order, the overall system samples at

$$t_n \equiv n \, \delta.$$
 (2)

In the above definitions, both n and n' are integers. It is also clear that the sample taken at time t_n originates from $ADC_{n \bmod P}$. We assume that the "integration time" or aperture width of each ADC is much shorter than δ , so that each sample can be treated as an instantaneous value.

Practical implementations of ADC interleaving often encounter mismatches between the ADCs, which can significantly degrade system performance. Following Roshanineshat (2023), we ignore bandwidth mismatches and focus on three primary types of mismatches: i) phase delay mismatches τ_p , ii) gain mismatches γ_p , and iii) offset mismatches α_p . Phase delay mismatches refer to timing deviations in the effective sampling instants of the ADCs, typically caused by differences in clock routing or circuitry delays across channels. Gain mismatches represent variations in the amplification factors of the ADCs, and offset mismatches denote differences in their baseline DC levels. Both gain and offset mismatches usually arise from manufacturing variations between individual ADCs. The combined effect of these mismatches is illustrated in Figure 1.

To model the sampled data from ADC_p in the presence of these mismatches, we use the following expression:

$$\tilde{f}_{p,n'} = \gamma_p f(n'\Delta + p\,\delta + \tau_p) + \alpha_p,\tag{3}$$

where the tilde ($\tilde{}$) denotes that the sampled data includes mismatch effects. Rewriting this in terms of the global interleaved sampling index n, we obtain:

$$\tilde{f}_n = \gamma_{n \bmod P} f(n \delta + \tau_{n \bmod P}) + \alpha_{n \bmod P}.$$
 (4)

To calibrate the system and correct these mismatches, we use a sinusoidal reference signal of known period T:

$$f(t) = A\cos(\Omega t) = \frac{A}{2} \left[e^{i\Omega t} + \text{C.C.} \right], \qquad (5)$$

where $\Omega \equiv 2\pi/T$ and "C.C." denotes the complex conjugate of the preceding term. The sampled/discretized version of this signal, affected by the mismatches in equation (4), is therefore given by

$$\tilde{f}_n = \gamma_{n \bmod P} \frac{A}{2} \left[e^{i\Omega(n\delta + \tau_{n \bmod P})} + \text{C.C.} \right] + \alpha_{n \bmod P}.$$
(6)

Throughout this paper, we define the discrete-time Fourier transform of the sampled data \tilde{f}_n as

$$\tilde{\mathcal{F}}_{\omega} = \sum_{n = -\infty}^{\infty} e^{-i\omega n\delta} \tilde{f}_n. \tag{7}$$

This formulation provides the basis for our calibration algorithm described in the following sections.

3. MATHEMATICAL DERIVATION

In this section, we derive the mathematical identities that form the foundation of our direct calibration algorithm to correct phase delay, gain, and offset mismatches. The key idea is to analyze the Fourier coefficients of the sampled sinusoidal reference signal, which encode the mismatch parameters in a structured way.

Substituting the sampled signal with mismatches from equation (6) into the definition of the Fourier transform in equation (7), we obtain

$$\tilde{\mathcal{F}}_{\omega} = \sum_{n=-\infty}^{\infty} e^{-i\omega n\delta} \left\{ \gamma_{n \bmod P} \frac{A}{2} \left[e^{i\Omega(n\delta + \tau_{n \bmod P})} + \text{C.C.} \right] + \alpha_{n \bmod P} \right\}$$
(8)

$$= \sum_{n'=-\infty}^{\infty} \sum_{p=0}^{P-1} e^{-i\omega(n'P+p)\delta} \left\{ \gamma_p \frac{A}{2} \left[e^{i\Omega[(n'P+p)\delta + \tau_p]} + \text{C.C.} \right] + \alpha_p \right\}$$
(9)

$$=\frac{A}{2}\sum_{n'=-\infty}^{\infty}e^{-i\omega n'P\delta+i\Omega n'P\delta}\sum_{p=0}^{P-1}\gamma_p\left[e^{-i\omega p\delta+i\Omega(p\delta+\tau_p)}+\text{C.C.}\right]+\sum_{n'=-\infty}^{\infty}e^{-i\omega n'P\delta}\sum_{p=0}^{P-1}e^{-i\omega p\delta}\alpha_p$$
(10)

$$= \frac{A}{2} \sum_{n'=-\infty}^{\infty} e^{-i(\omega-\Omega)n'\Delta} \sum_{p=0}^{P-1} \gamma_p \left[e^{-i(\omega-\Omega)p\delta + i\Omega\tau_p} + \text{C.C.} \right] + \sum_{n'=-\infty}^{\infty} e^{-i\omega n'\Delta} \sum_{p=0}^{P-1} e^{-i\omega p\delta} \alpha_p$$
(11)

The two infinite sums over n' in equation (11) are non-zero only if $\Delta(\omega - \Omega) = 2\pi m$ and $\Delta\omega = 2\pi m'$, respectively, for some integers m and m'. Letting $\Omega_{\Delta} \equiv 2\pi/\Delta$, equation (11) simplifies to

$$\tilde{\mathcal{F}}_{\omega} = \frac{A}{2}\delta(\omega - \Omega - m\Omega_{\Delta}) \sum_{p=0}^{P-1} \gamma_p \left[e^{-i(\omega - \Omega)p\delta + i\Omega\tau_p} + \text{C.C.} \right] + \delta(\omega - m'\Omega_{\Delta}) \sum_{p=0}^{P-1} e^{-i\omega p\delta} \alpha_p.$$
 (12)

Assuming that Ω is not an integer multiple of Ω_{Δ} , the two types of nonzero Fourier coefficients are:

$$\tilde{\mathcal{F}}_{\Omega+m\Omega_{\Delta}} = \frac{A}{2} \sum_{p=0}^{P-1} e^{-im\Omega_{\Delta}p\delta} \gamma_p e^{i\Omega\tau_p} = \frac{A}{2} \sum_{p=0}^{P-1} e^{-2\pi imp/P} \gamma_p e^{i\Omega\tau_p}, \tag{13}$$

$$\tilde{\mathcal{F}}_{m'\Omega_{\Delta}} = \sum_{p=0}^{P-1} e^{-im'\Omega_{\Delta}p\delta} \alpha_p = \sum_{p=0}^{P-1} e^{-2\pi im'p/P} \alpha_p. \tag{14}$$

To derive our calibration algorithm, according to equation (13), we define

$$\tilde{\mathcal{R}}_m \equiv \frac{\tilde{\mathcal{F}}_{\Omega + m\Omega_{\Delta}}}{A/2} \tag{15}$$

as the $dimensionless\ ratio$ of the non-zero coefficients and A/2, and

$$\Gamma_p \equiv \gamma_p e^{i\Omega \tau_p} \tag{16}$$

as the complex gain for ADC_p on the reference signal, $f(t) = A\cos(\Omega t)$, which encapsulates both gain and phase delay mismatches. According to equation (14), it is convenient to define

$$\tilde{\mathcal{A}}_m \equiv \tilde{\mathcal{F}}_{m\Omega\Lambda},\tag{17}$$

where we drop the prime for notational simplicity. With these definitions, equations (13) and (14) reduce to

$$\tilde{\mathcal{R}}_m = \sum_{p=0}^{P-1} e^{-2\pi i m p/P} \Gamma_p, \tag{18}$$

$$\tilde{\mathcal{A}}_m = \sum_{p=0}^{P-1} e^{-2\pi i m p/P} \alpha_p. \tag{19}$$

Equations (18) and (19) are the main result of this paper. They show that $\tilde{\mathcal{R}}_m$ and $\tilde{\mathcal{A}}_m$ are simply the discrete Fourier transforms (DFTs) of the complex gain Γ_p and the offset mismatch α_p , respectively. These identities generalize equation (7) in Shen et al. (2022). They can also be seen as a special cases of a standard decomposition commonly used in parallelizing one-dimensional fast Fourier transforms (FFTs).

P	N_{δ}	$N_T N_\delta$	$N_T N_\delta/P$	$RMS(\hat{\gamma}_p - \gamma_p)$	$RMS(\hat{\tau}_p - \tau_p)$	$RMS(\hat{\alpha}_p - \alpha_p)$
2	2	2	1	1.896e+00	9.435e-04	8.916e-01
2	3	6	3	3.237e-16	3.019e-18	2.614e-16
2	4	4	2	7.472e-01	3.395e-03	4.763e-17
2	5	10	5	1.755e-16	1.238e-18	1.870e-16
2	6	6	3	7.850e-17	2.719e-18	1.376e-16
2	7	14	7	1.755e-16	2.892e-18	6.090e-17
2	8	8	4	0.000e+00	1.333e-18	2.314e-17
2	9	18	9	1.570e-16	3.803e-18	1.972e-16
2	10	10	5	1.755e-16	8.606e-19	3.035e-17
2	11	22	11	2.220e-16	1.516e-18	1.097e-17
3	2	6	2	8.617e-01	8.668e-04	9.363e-17
3	3	3	1	1.431e+00	3.351e-03	8.124e-01
3	4	12	4	6.410e-17	5.056e-18	4.446e-16
3	5	15	5	5.477e-16	4.190e-18	4.502e-16
3	6	6	2	6.277e-01	5.652e-03	1.540e-16
3	7	21	7	1.433e-16	5.274e-18	1.152e-16
3	8	24	8	1.923e-16	5.054e-18	2.873e-16
3	9	9	3	2.311e-16	2.731e-18	1.622e-16
3	10	30	10	1.813e-16	6.862e-18	2.125e-16
3	11	33	11	1.282e-16	2.783e-18	1.156e-16
4	2	4	1	8.975e-01	7.465e-04	9.439e-01
4	3	12	3	1.561e-02	5.026e-05	2.263e-16
4	4	4	1	1.091e+00	5.208e-03	7.265e-01
4	5	20	5	2.989e-16	6.033e-18	5.752e-16
4	6	12	3	2.289e-16	3.965e-18	1.597e-16
4	7	28	7	5.118e-16	9.702e-18	2.091e-16
4	8	8	2	7.197e-01	7.778e-03	4.284e-17
4	9	36	9	2.989e-16	7.416e-18	1.901e-16
4	10	20	5	2.776e-16	8.162e-18	1.516e-16
4	11	44	11	2.719e-16	3.811e-18	2.730e-16
5	2	10	2	8.991e-01	7.319e-04	2.340e-16
5	3	15	3	1.300e-01	3.390e-04	8.141e-16
5	4	20	4	4.699e-02	1.841e-04	6.474e-16
5	5	5	1	1.005e+00	4.815e-03	7.099e-01
5	6	30	6	4.578e-16	8.607e-18	8.437e-16
5	7	35	7	5.371e-16	1.520e-17	4.529e-16
5	8	40	8	3.179e-16	1.006e-17	2.153e-16
5	9	45	9	5.088e-16	1.592e-17	3.906e-16
5	10	10	2	6.321e-01	8.801e-03	8.631e-17
5	11	55	11	2.809e-16	1.028e-17	1.288e-16
6	2	6	1	8.961e-01	6.987e-04	9.520e-01
6	3	6	1	7.023e-01	2.004e-03	7.973e-01
6	4	12	2	8.840e-01	3.830e-03	2.891e-16
6	5	30	5	1.080e-02	4.614e-05	6.736e-16
6	6	6	1	1.032e+00	8.547e-03	6.682e-01
6	7	42	7	6.362e-16	1.458e-17	6.956e-16
6	8	24	4	3.654e-16	4.031e-18	2.304e-16
6	9	18	3	2.311e-16	6.628e-18	2.286e-16
6	10	30	5	2.794e-16	7.599e-18	4.026e-16
6	11	66	11	7.166e-16		
	11	00	11	7.100e-10	1.052e-17	2.740e-16

Table 1. Summary of a representative set of numerical experiments on recovering mismatch parameters in a P-ADC interleaving system. Here, P is the number of interleaved ADCs; N_{δ} is the total number of samples per reference signal period across all ADCs; and $N_T N_{\delta} = \text{LCM}(P, N_{\delta})$ is the minimum total number of sampling points required so that each ADC receives an equal number of samples. Consequently, $N_T N_{\delta}/P$ is the number of samples acquired by each individual ADC. For each experiment, we randomly generate the ground-truth mismatch parameters $\hat{\gamma}_p$, $\hat{\tau}_p$, and $\hat{\alpha}_p$, then sample synthetic data and solve for the recovered values γ_p , τ_p , and α_p using equations (20) and (21). We highlight the results in blue when both conditions $N_{\delta} > P$ and $N_T N_{\delta} \geq 3P$ are satisfied, which meets the theoretical requirements for accurately recovering all mismatch parameters. Otherwise, if only $N_T N_{\delta} \geq 2P$ is satisfied, the results are shown in green, indicating configurations sufficient for recovering offset mismatches, but not necessarily gain or phase delay mismatches.

Since both $\tilde{\mathcal{R}}_m$ and $\tilde{\mathcal{A}}_m$ are directly computable from the Fourier transform of the sampled data \tilde{f}_n , we can recover Γ_p and α_p by applying the inverse DFT:

$$\Gamma_p = \text{DFT}^{-1} \tilde{\mathcal{R}}_m \equiv \frac{1}{P} \sum_{p=0}^{P-1} e^{2\pi i m p/P} \tilde{\mathcal{R}}_m , \qquad (20)$$

$$\alpha_p = \mathrm{DFT}^{-1} \tilde{\mathcal{A}}_m \equiv \frac{1}{P} \sum_{p=0}^{P-1} e^{2\pi i m p/P} \tilde{\mathcal{A}}_m \,. \tag{21}$$

The mismatches can then be solved by:

Gain mismatch:
$$\gamma_p = |\Gamma_p|$$
 (22)

Phase delay mismatch:
$$\tau_p = \arg(\Gamma_p)/\Omega$$
 (23)

Offset mismatch:
$$\alpha_p$$
 (computed directly) (24)

These quantities can be used to correct for mismatches either through hardware adjustment or post-processing. The ability to solve for all mismatch parameters in closed form makes this calibration algorithm both efficient and scalable, especially in high-speed interleaved systems with many ADC cores.

4. MINIMAL SAMPLING REQUIREMENT

Equations (18) and (19) provide deterministic relations between the measured Fourier coefficients and the mismatch parameters. In the absence of noise, and with a sufficient number of samples, all mismatch parameters can be solved exactly, limited only by machine precision. This raises two interesting questions: i) What is the minimal number of sampling points per reference signal period T required to recover all mismatch parameters in a P-ADC interleaving system? ii) For a fixed number of sampling points per period N_{δ} , how many ADCs P can be interleaved while still enabling accurate calibration?

Throughout this section, we assume that the calibration signal frequency $\Omega = 2\pi/T$ is not an integer multiple of the interleaved sampling frequency $\Omega_{\Delta} = 2\pi/\Delta$. As discussed in the last section, this ensures that $\tilde{\mathcal{R}}_m$ and $\tilde{\mathcal{A}}_m$ do not mix. We begin by analyzing the recovery of offset mismatches α_p . To solve for each α_p individually, we must ensure that each ADC samples the signal an equal number of times. This occurs when the total number of samples is a multiple of the least common multiple (LCM), i.e.,

$$N_T N_{\delta} = \text{LCM}(P, N_{\delta}),$$
 (25)

where N_{δ} is the number of samples taken per reference signal period T across the entire interleaved system, and N_T is the number of periods required to achieve balanced sampling across all P ADCs. As long as $N_T N_{\delta} \geq 2P$, each ADC contributes at least two samples per period, which is sufficient to solve for the DC offset values α_p to machine accuracy, even if the signal is not Nyquist-sampled.

Recovering the gain γ_p and phase delay τ_p mismatches requires stricter conditions. To capture meaningful phase information, the system must have more samples per period than ADCs, i.e., $N_{\delta} > P$. Additionally, we require at least $N_T N_{\delta} \geq 3P$ total samples so that the system of equations has sufficient degrees of freedom to reliably solve for both amplitude and phase distortions.

Table 1 summarizes a set of numerical experiments that illustrate these criteria. Each experiment randomly generates a ground-truth set of mismatches $\hat{\gamma}_p$, $\hat{\tau}_p$, and $\hat{\alpha}_p$, and attempts to recover them by applying equations (20) and (21) to synthetic sampled data. The table reports reconstruction root-mean-square (RMS) errors, $\text{RMS}(\hat{\gamma}_p - \gamma_p)$, $\text{RMS}(\hat{\tau}_p - \tau_p)$, and $\text{RMS}(\hat{\alpha}_p - \alpha_p)$, under different configurations of P and N_{δ} .

The results are color-coded to show the sufficiency of the sampling configuration:

- Blue entries indicate that both $N_{\delta} > P$ and $N_T N_{\delta} \geq 3P$ are satisfied, meeting the theoretical minimum for solving all mismatch parameters (phase, gain, and offset).
- Green entries mark cases where $N_T N_{\delta} \geq 2P$ but $N_{\delta} \leq P$, satisfying only the condition for solving the offset mismatches α_p .

Determining the minimal N_{δ} (samples per period) depends on the relationship between P and N_{δ} . However, a particularly elegant and efficient configuration occurs when $N_{\delta} = P + 1$. In this case, because P and P + 1 are *coprime*, we have

$$N_T N_{\delta} = \text{LCM}(P, N_{\delta}) = P(P+1),$$
 (26)

which guarantees that each ADC samples the reference signal P+1 times, evenly distributed across P periods. This yields exactly $P(P+1) \geq 3P$ samples, satisfying all requirements to solve for gain, delay, and offset mismatches.

5. CONVERGENCE PROPERTIES

When using the minimal number of samples required for mismatch recovery, any noise in the system can significantly degrade the accuracy of the solution. Figure 2 illustrates how phase delay, gain, and offset mismatches, as well as noise, affect the frequency spectrum of the sampled signal before calibration. The left panels show spurious peaks appear at frequency offsets of $\Omega + m\Omega_{\Delta}$ as a result of phase delay mismatches. The right panels show, in the presence of noise, these features remain visible but are partially masked, motivating the need for oversampling strategies to enhance the signal-to-noise ratio (SNR) in the calibration process.

To mitigate noise, it is essential to oversample the reference signal so that noise effects can be averaged out. We consider two main strategies to increase sampling redundancy. First, the number of samples per period, N_{δ} ,

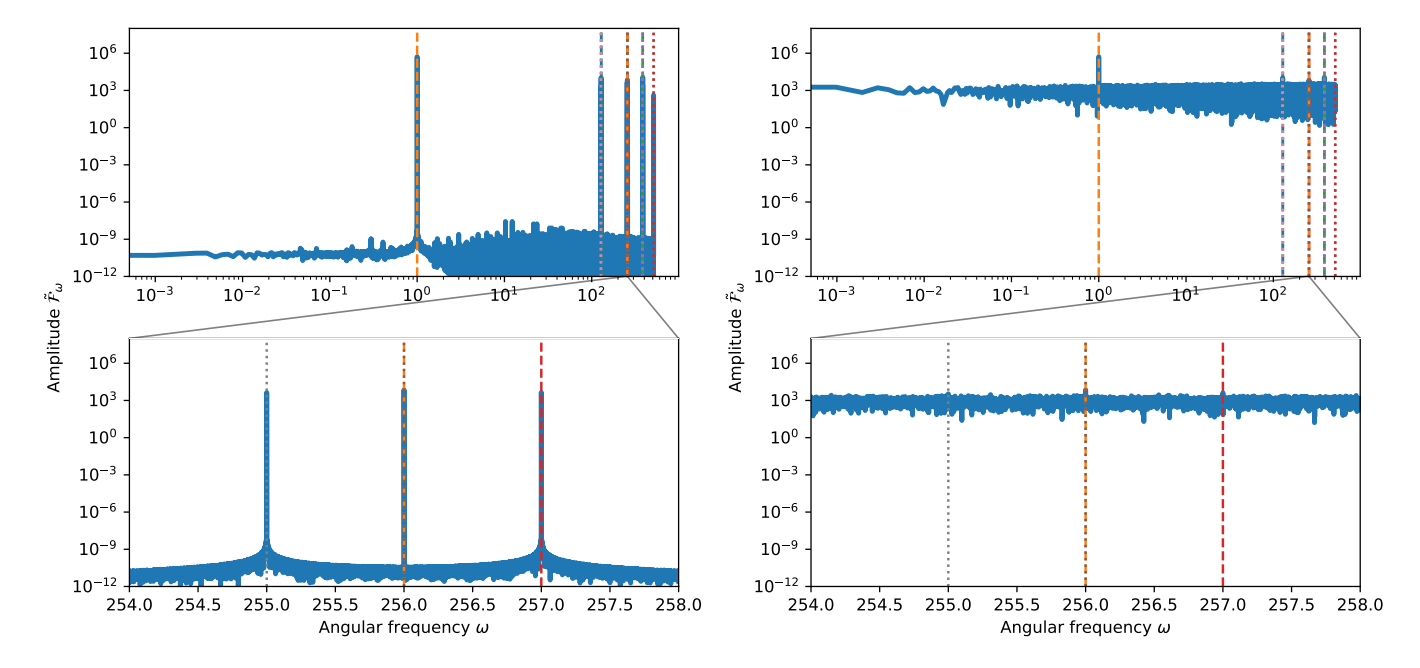


Figure 2. (Left) Frequency spectrum of the signal before applying the proposed direct calibration algorithm, illustrating the effects of phase delay, gain, and offset mismatches in a 4-ADC interleaving system. Dashed and dotted vertical lines in different colors mark the frequencies at $\Omega + m\Omega_{\Delta}$ (see equation (13)) and $m'\Omega_{\Delta}$ (see equation (14)), respectively. The top panel shows the full spectrum across a broad range of angular frequencies, while the bottom panel provides a zoomed-in view of a specific band, clearly revealing spurious peaks primarily caused by phase delay mismatches. (Right) Same as the left, but with additive noise. The noise level is comparable to that of the reference signal. Although the spurious peaks remain visible, their amplitudes are partially masked by the noise.

can be increased to oversample the reference waveform in time. For a physical P-ADC system where P and Δ are fixed, this can be achieved by tuning the reference signal's frequency $\Omega=2\pi/T$ so that its period satisfies $T=N_\delta\delta$. It is also important to note that real ADCs have finite integration times. Increasing T helps ensure that this finite integration time remains negligible in the calibration procedure. Second, the number of sampled periods, N_T , can be increased while keeping N_δ fixed. This allows for temporal averaging across many cycles of the reference signal.

In our numerical experiments shown in Table 1 and Figure 3, we fix the interleaved sampling interval δ to represent a hardware constraint. The actual value is not important, but for completeness, our numerical experiment uses $\delta = 2\pi/1024$. The number of interleaved ADCs, P, determines the sampling interval for each ADC. We then vary N_{δ} and N_{T} to investigate how recovery accuracy depends on total sampling.

Figure 3 quantifies the convergence behavior of our calibration algorithm. In the left column, we fix $N_T = 256$ and vary N_{δ} ; in the right column, we fix $N_{\delta} = 256$ and vary N_T . Each panel reports the RMS error in recovering the mismatch parameters: phase delay τ_p , gain γ_p , and offset α_p , under three different noise conditions:

Top row (no noise): When $N_{\delta} \lesssim 200$, the number of samples is below the theoretical minimum, and all recovered parameters exhibit significant errors. Once

 $N_{\delta} \gtrsim 200$, the error in γ_p and α_p drops to machine precision, consistent with the deterministic predictions of our theory. However, even in this regime, the phase delay τ_p continues to scale linearly with N_{δ} . This is explained by the fact that increasing N_{δ} lowers the reference frequency Ω , and since $\tau_p = \arg(\Gamma_p)/\Omega$, small phase errors in Γ_p get amplified. When varying N_T at fixed N_{δ} , the errors in γ_p and α_p remain flat, while τ_p still exhibits increasing error due to its dependence on total integration time.

Middle row (additive amplitude noise): Errors in γ_p and α_p scale approximately as $1/\sqrt{N_\delta}$ and $1/\sqrt{N_T}$, reflecting classical statistical averaging. However, for τ_p , the scaling with N_δ becomes worse due to the additional $\Omega^{-1} \propto N_\delta$ factor, resulting in τ_p errors scaling roughly as $\sqrt{N_\delta}$. When N_T increases (right column), all mismatch parameters benefit equally from temporal averaging and scale as $1/\sqrt{N_T}$.

Bottom row (sampling jitter): When noise affects the sampling times directly (timing jitter), the error in τ_p dominates and decreases approximately as $1/\sqrt{N_\delta}$. Interestingly, errors in γ_p and α_p decrease faster, with scaling close to $1/N_\delta^{3/2}$. This behavior likely arises because jitter impacts phase recovery most directly, while the amplitude and offset terms average out more efficiently.

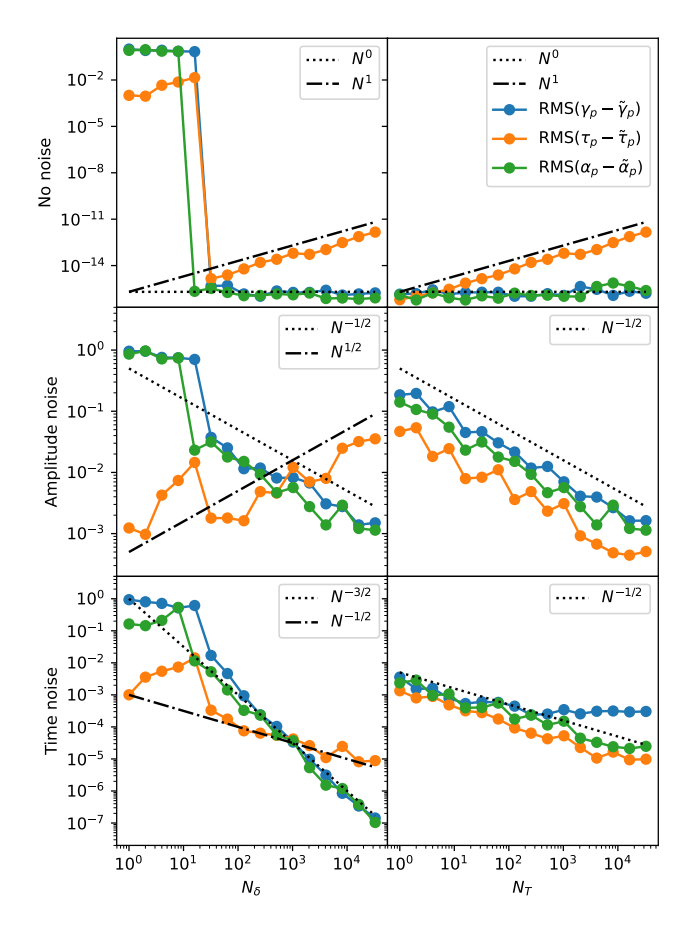


Figure 3. Convergence properties of the proposed direct calibration algorithm as a function of the number of samples. (Left column) The number of periods is fixed at $N_T=256$, while the number of samples per period N_δ is varied. (Right column) The number of samples per period is fixed at $N_\delta=256$, while the number of periods N_T is varied. Colored circles indicate the RMS errors in recovering each mismatch parameter: phase delay τ_p , gain γ_p , and offset α_p . The dotted and dash-dotted lines show reference slopes for ideal scaling behavior, allowing comparison to theoretical convergence rates. These plots demonstrate that different mismatch parameters exhibit distinct but predicted convergence characteristics. See section 5 for details.

These results suggest that while gain and offset mismatches can be reliably recovered at relatively low SNRs, phase delay recovery requires higher sampling density and cleaner reference signals to achieve comparable accuracy.

In all cases, the constants of proportionality in the error scaling depend on the amplitude and nature of the noise. In physical systems, such noise is determined by factors such as thermal fluctuations, system temperature, and clock phase jitter. As a practical guideline, we recommend performing a system-specific calibration sensitivity analysis to determine the minimal values of

 N_{δ} and N_{T} required to meet the desired accuracy thresholds for each mismatch parameter. This approach balances hardware constraints and calibration precision, and ensures robust operation of interleaved ADC systems in noisy environments.

6. A DIRECT CALIBRATION ALGORITHM

We now present an efficient direct calibration algorithm to recover gain, phase delay, and offset mismatches $(\gamma_p, \tau_p, \text{ and } \alpha_p)$ in a P-ADC interleaving system with computation complexity $\mathcal{O}(N \min(\log N, P))$.

The hardware configuration specifies the number of interleaving ADCs P and their sampling interval Δ , which determines the interleaved sampling interval $\delta = \Delta/P$. To perform calibration, we sample a known sinusoidal reference signal with angular frequency Ω at period $T=N_\delta\delta$. Here, N_δ is the number of samples per period across all ADCs, and N_T is the number of full signal periods sampled. This results in a total of $N=N_\delta N_T$ sampled points.

Our goal is to extract the Fourier coefficients $\mathcal{F}_{\Omega+m\Omega_{\Delta}}$ and $\tilde{\mathcal{F}}_{m\Omega_{\Delta}}$ from the sampled data \tilde{f}_n , where $\Omega_{\Delta}=2\pi/\Delta$. These coefficients are then used to compute $\tilde{\mathcal{R}}_m$ and $\tilde{\mathcal{A}}_m$, from which the complex gains $\Gamma_p=\gamma_p e^{i\Omega\tau_p}$ and offsets α_p are recovered via inverse discrete Fourier transforms, as given in equations (20) and (21).

To compute the Fourier transform of the sampled signal, one may use a Fast Fourier Transform (FFT) or a direct (matrix-based) Discrete Fourier Transform (DFT), depending on the problem size. If the total number of samples N is large $(N\gg P)$, FFT provides a faster solution. For small-scale problems with modest P, DFT may be efficient and more flexible for selecting arbitrary frequencies. Once Γ_p and α_p are computed, we extract the gain and phase mismatches using $\gamma_p = |\Gamma_p|$ and $\tau_p = \arg(\Gamma_p)/\Omega$.

The entire procedure is summarized in Algorithm 1. Once the mismatch parameters are recovered, corrections can be applied in hardware by adjusting ADC clocks or digital compensation blocks, or in software during post-processing if the mismatches are small and stable. Because the algorithm is fast and lightweight, it can be run repeatedly to track and correct for slow mismatch drifts during operation, enabling robust, ongoing calibration with minimal overhead.

7. DISCUSSION AND CONCLUSION

In this paper, we have presented a novel direct calibration algorithm to correct phase delay, gain, and offset mismatches in ADC interleaving systems. The algorithm is based on a deterministic analysis using Fourier transforms of a sinusoidal reference signal, enabling efficient and accurate extraction of mismatch parameters from the frequency-domain representation of the sampled data. By avoiding iterative search or optimization, our method achieves both computational efficiency and mathematical transparency.

Algorithm 1: The proposed direct Fourier-based calibration algorithm for recovering gain, phase delay, and offset mismatches in interleaved ADC systems. Note that $m = 0, 1, \ldots, P - 1$.

```
Result: \alpha_p, \gamma_p, and \tau_p for p = 0, 1, \dots, P-1
while need calibration do
         \tilde{f}_n \leftarrow N samples from reference signal \cos(\Omega t);
        if 2P > 5 \log N then
                \tilde{\mathcal{F}}_{\omega} \leftarrow \operatorname{FFT} \tilde{f}_n;
        else
               \tilde{\mathcal{F}}_{\omega} \leftarrow \mathrm{DFT}\tilde{f}_n \text{ for } \omega = \Omega + m\Omega_{\Delta} \text{ or } m\Omega_{\Delta};
        \tilde{\mathcal{R}}_m \leftarrow \tilde{\mathcal{F}}_{\Omega+m\Omega_{\Delta}}/(A/2);
        \tilde{\mathcal{A}}_m \leftarrow \tilde{\mathcal{F}}_{m\Omega_{\Delta}};
        if P \gg 5 \log P then
                \Gamma_p \leftarrow \text{FFT}^{-1} \tilde{\mathcal{R}}_m;
                 \alpha_p \leftarrow \text{FFT}^{-1} \tilde{\mathcal{A}}_m;
                 \Gamma_p \leftarrow \mathrm{DFT}^{-1} \tilde{\mathcal{R}}_m;
               \alpha_p \leftarrow \mathrm{DFT}^{-1} \tilde{\mathcal{A}}_m;
        \gamma_p \leftarrow |\Gamma_p|;
        \tau_p \leftarrow \arg(\Gamma_p)/\Omega;
        adjust hardware and/or post-process parameters
           according to \tau_p, \gamma_p, and \alpha_p;
\quad \mathbf{end} \quad
```

We have demonstrated that the mismatch parameters can be recovered from the observed signal. This enables flexible implementation strategies: the mismatch corrections can be applied in *hardware*, through adjustments to ADC sampling clocks, gain amplifiers, or DC offset registers; in *software*, by compensating for the recovered mismatches during post-processing; or in a *hybrid* approach, where coarse corrections are handled in hardware and fine-tuning is performed in software post-processing. Because our algorithm is fast and lightweight, it can be invoked repeatedly to track slow drift in mismatch parameters, which is important for long-duration observations or thermally varying environments.

We validated the algorithm through a series of numerical experiments that demonstrate the minimal sampling requirements for robust calibration and the convergence behavior under different noise models. In particular, we showed that phase delay mismatch recovery is more sensitive to sampling density and noise compared to gain and offset mismatches in our setup.

The proposed approach is well-suited for high-speed, high-precision applications such as radio astronomy and VLBI. VLBI systems often rely on tightly synchronized, interleaved ADC architectures to achieve extremely high bandwidths. Spurious tones and spectral leakage from uncorrected mismatches can compromise image reconstruction and astrometric precision. Recent work by the EHT collaboration (e.g., Event Horizon Telescope Collaboration et al. 2022) has emphasized the need for calibration strategies that scale with increasing ADC count and bandwidth. Our method provides a deterministic and scalable solution to this challenge. By enabling reliable calibration with arbitrary numbers of interleaved ADCs, it opens a pathway to even broader bandwidths and finer time resolution in next-generation instruments.

Several promising avenues exist for extending this work. First, implementing the algorithm in FPGA or real-time DSP systems will allow on-the-fly mismatch correction, enabling real-time calibration in operational environments. Second, incorporating feedback mechanisms to track slow drifts in mismatch parameters (e.g., due to thermal changes) could allow the system to maintain calibration autonomously over time. Third, extending the method to handle non-sinusoidal or multi-tone calibration signals could facilitate mismatch recovery without interrupting the science data stream. Finally, studying how ADC quantization influences mismatch recovery will be crucial for low-bit-depth systems. In particular, we propose analyzing how quantization and noise levels jointly limit the maximum phase mismatch that can be reliably corrected in software.

The direct calibration algorithm presented in this work offers an efficient, deterministic, and scalable solution to correct ADC interleaving mismatches. Its low computational overhead, compatibility with hardware and software workflows, and high accuracy make it an attractive approach for future high-throughput data acquisition systems. In the context of radio astronomy and VLBI, it contributes to next-generation calibration pipelines, allowing for wider bandwidths, improved signal fidelity, and enhanced scientific capabilities.

REFERENCES

```
2010, 56GSa/s 8-bit Analog-to-Digital Converter, Fujitsu Electronics America, Inc. https://www.fujitsu.com/tw/Images/56G_ADC_FactSheet.pdf
Dewdney, P. E., Hall, P. J., Schilizzi, R. T., & Lazio, T. J. L. W. 2009, IEEE Proceedings, 97, 1482, doi: 10.1109/JPROC.2009.2021005
```

```
Elbornsson, J., Gustafsson, F., & Eklund, J.-E. 2005, IEEE Transactions on Circuits and Systems I: Regular Papers, 52, 465. https://ieeexplore.ieee.org/document/1406174 Event Horizon Telescope Collaboration, Akiyama, K., Alberdi, A., et al. 2019a, ApJL, 875, L2, doi: 10.3847/2041-8213/ab0c96

—. 2019b, ApJL, 875, L3, doi: 10.3847/2041-8213/ab0c57
```

- 2022, ApJL, 930, L13, doi: 10.3847/2041-8213/ac6675
 Hu, M., & Yi, P. 2022, Applied Sciences, 12, doi: 10.3390/app122111029
- Iguchi, S., Kawaguchi, N., Okumura, S. K., & Sunada, K. 2003, in Astronomical Society of the Pacific Conference Series, Vol. 306, New technologies in VLBI, ed. Y. C. Minh, 161–176
- Jiang, H., Yu, C.-Y., Chen, M., & Liu, M. 2020, PASP, 132, 085001, doi: 10.1088/1538-3873/ab99ce
- Manganaro, G., & Robertson, D. 2015, Analog Dialogue, 49. https://www.analog.com/en/resources/ analog-dialogue/articles/interleaving-adcs.html
- Patel, N. A., Wilson, R. W., Primiani, R., et al. 2014, Journal of Astronomical Instrumentation, 3, 1450001, doi: 10.1142/S2251171714500019

- Reeder, R., Looney, M., Hand, J., et al. 2005, Analog Dialogue, 39, 7.
 - https://www.analog.com/en/resources/analog-dialogue/articles/multichannel-a-d-converters.html
- Roshanineshat, A. 2023, PhD thesis, University of Arizona
 Shen, H., Blaq, A., John, D., & Cardiff, B. 2022, IEEE
 Transactions on Circuits and Systems I: Regular Papers,
 70, 1110. https://ieeexplore.ieee.org/document/9991970
- Sjöland, H., & Palm, M. 2022, Calibration technique for time-interleaved analog-to-digital converters. https://patents.justia.com/patent/11323128
- Sundström, L., Mastantuono, D., & Palm, M. 2023, Time-interleaved analog-to-digital converter. https://patents.justia.com/patent/11545989